C. R. Physique 11 (2010) 54–67

Contents lists available at ScienceDirect

Comptes Rendus Physique

www.sciencedirect.com

Propagation and remote sensing / Propagation et télédétection

Radar monitoring of a wake vortex: Electromagnetic reflection of wake turbulence in clear air

Imagerie Radar des tourbillons de sillage : Réflexion électromagnétique des turbulences de sillage en air clair

Frédéric Barbaresco [a,*], Uwe Meier [b]

[a] *Thales Air Systems, Département Stratégie Technologie et Innovation, Unité Surface Radar, Hameau de Roussigny, 91470 Limours, France*
[b] *Thales Defence Deutschland GmbH, Land & Joint Division, Pforzheim, Germany*

ARTICLE INFO

Article history:
Available online 25 February 2010

Keywords:
Wake vortex
Wake turbulence
Radar monitoring in clear air

Mots-clés :
Tourbillons de sillage
Turbulences de sillage
Imagerie radar en air clair

ABSTRACT

This article deals with X-band radar trial campaigns in 2006 and 2007 at Orly Airport, and in June 2008 at Paris-CDG Airport. An X-band Doppler radar has been deployed to assess short range (inferior to 2000 m) wake vortex monitoring capabilities in all weather conditions (dry and wet conditions). Recorded data have been correlated with electromagnetic and fluid mechanical models of wake turbulences for better and more accurate understanding of roll-up radar cross section (RCS) and Doppler signature.

© 2010 Académie des sciences. Published by Elsevier Masson SAS. All rights reserved.

RÉSUMÉ

Cet article traite des campagnes de mesures radar bande X de 2006 et 2007 sur l'Aéroport Orly et juin 2008 sur l'Aéroport de Paris-CDG. Un radar Doppler bande X a été déployé pour évaluer les capacités d'imagerie à courte portée (inférieure à 2000 m) des tourbillons de sillage suivant différentes conditions météorologiques (air clair et pluie). Les données enregistrées ont été corrélées avec les modèles électromagnétiques et les modèles de mécaniques des fluides des turbulences de sillage pour une meilleure compréhension de la surface équivalente radar (SER) des rouleaux et de leur signature Doppler.

© 2010 Académie des sciences. Published by Elsevier Masson SAS. All rights reserved.

1. Introduction

An aircraft creates wake vortices in different flying phases. To avoid jeopardizing flight safety by wake vortices encounters, time/distance separations have been conservatively increased, thus restricting runway capacity. The concern is higher during taking off and landing phases, as aircrafts are less easy to maneuver. These vortices usually dissipate quickly (decay due to air turbulence or transport by cross-wind), but most airports operate for the safest scenario, which means the interval between aircraft taking off or landing often amounts to several minutes. However, with the aid of accurate wind data and precise measurements of the wake vortex, more efficient intervals can be set, particularly when weather conditions are stable. Depending on traffic volume, these adjustments can generate capacity gains which have major commercial benefits.

* Corresponding author.
E-mail addresses: frederic.barbaresco@thalesgroup.com (F. Barbaresco), uwe.meier@de.thalesgroup.com (U. Meier).

1631-0705/$ – see front matter © 2010 Académie des sciences. Published by Elsevier Masson SAS. All rights reserved.
doi:10.1016/j.crhy.2010.01.001

With the steady increase in air traffic, civil aviation authorities are under continuous pressure to increase aircraft handling capacity. One potential approach is to reduce these separation distances between aircraft at take-off and landing without compromising safety. ICAO safety provision for aircraft separation criteria has been defined in the early 1970s and has, since then, served to maintain acceptable standards of wake vortex safety. Such a standard is based on fixed distance or time separation between aircraft according to their respective category, without indexing according to weather conditions (cross-wind, eddy dissipation). These ICAO Standard Safety separations are very conservative.

Wake vortices are a natural by-product of lift generated by aircraft and can be considered as two horizontal tornados trailing after the aircraft. A trailing aircraft exposed to the wake vortex turbulence of a lead aircraft can experience an induced roll moment (bank angle) that is not easily corrected by the pilot or the autopilot. However, these distances can be safely reduced with the aid of smart planning techniques of future Wake Vortex Advisory Systems based on wake vortex detection/monitoring and wake vortex prediction (mainly transport estimation by cross-wind), significantly increasing airport capacity. This limiting factor will be significantly accentuated soon with the arrival of new heavy aircrafts: the Airbus A380 and the new stretched version of Boeing B747-8. Very recently, the ICAO has recommended for A380 new safety separations larger than those already applied for the B747 and the UK authorities have announced in November 2006, the introduction of "Super Wake Vortex Category" for Airbus A380.

The study detailed in the article is one part of a larger project with objective to develop a Ground/Board Collaborative Wake Vortex Advisory System that would allow variable aircraft separation distances, as opposed to the fixed distances presently applied at airports. This Wake Vortex Advisory System should integrate wake vortex detection/monitoring sensors used in decision-support system and procedures that will help air traffic controllers to decide how long the intervals should be.

Candidate sensors are based on low cost Lidar & Radar technologies (1.5-micron VLS14 Pulsed Lidar from LEOSPHERE & ONERA and X-band Doppler Radar BOR-A550 from THALES). Capabilities of these sensors to continually monitor wake turbulence on runways or at the ILS interception area are studied. Wake turbulence data could be in fine combined with meteorological data & Wake Vortex Predictor [39–42] to generate recommendations for intervals, which are displayed on the air traffic controller's screen. Currently, Lidar sensors are used for wake vortex measurements, but their performance could be limited in adverse weather like rain or fog. On the other hand, radar is a good complementary sensor, which can be used for turbulence remote sensing as well (wake vortex, wind-shear, micro-bursts). It is able to work in different weather conditions like fog, rain, wind, and dry air.

To assess maturity and capability of an X-band radar to monitor wake roll-ups in all weather conditions, radar data have been collected in different weather conditions [27–34]. A Doppler X-band Radar, BOR-A 550, was deployed near runway at Orly airport and just under ILS interception area (entering of the glide path) in 2006 & 2007. Additional trials have taken place on Paris-CDG Airport in June 2008 to benchmark Lidar & Radar Technologies. Continuous detection, characterization (strength assessment: circulation in m^2/s), and profiling (age: young/mature/old/decaying) capabilities of wake vortices up to a range of 2000 m have been proved in clear air and rainy weather. Recorded data have been correlated with electromagnetic and fluid mechanical models of wake turbulences for better and more accurate understanding of roll-ups radar cross section (RCS) and Doppler signature. 0.2 m/s Doppler resolution was used with regularized high Doppler resolution techniques to characterize the wake vortex speed distribution in detail. X-band radar has been proved to be a full-fledged alternative, which can make a significant contribution to a wake vortex alert system, but to achieve as much reliability as possible, collaborative electro-optical & electromagnetic sensors solution is envisaged encapsulated in a Wake Vortex Advisory System. These sensors could be used to permanently monitor wake turbulence on runways. Wake turbulence data from sensors will be combined with meteorological nowcasting and forecasting data and a wake vortex predictor [39–42] to generate recommendations for intervals, which will be displayed on the air traffic controller's screen.

2. Physics of wake vortex hazards

In this section, we will describe physics of the wake vortex hazard and the origin of wake vortex radar cross section in clear air. These elements are important to analyze and understand Doppler radar signature.

The wake vortices shed by an aircraft are a natural consequence of its lift. The wake flow behind an aircraft can be described by near field and far field characteristics. In the near field small vortices emerge from that vortex sheet at the wing tips and at the edges of the landing flaps.

After roll-up the wake generally consists of two coherent counter-rotating swirling flows, like horizontal tornadoes, of about equal strength: the aircraft wake vortices.

Fluid dynamic of wake turbulence is modeled by the Navier equations, that have been expressed in a new form by Jean Leray [1–3] that can be used for radar wake vortex signature analysis because the new Leray's equation only depends on velocity u and no longer on pressure p. At $t = 0$, if we assume that $\operatorname{div} u = 0$, then velocity u is driven by: $\frac{du}{dt} = -(u \cdot \nabla)u + \nu \Delta u - \nabla p$. Then, pressure $p = p(t, x)$ has to be identified, such that divergence of u remains equal to zero. Leray has noticed that if we write $\operatorname{div}[(u \cdot \nabla)u + \nabla p] = \operatorname{tr}(\nabla u)^2 + \Delta p$, then $\operatorname{div}[(u \cdot \nabla)u + \nabla p] = 0$, if and only if $\Delta p = -\operatorname{tr}(\nabla u)^2$. At this step, Leray has used solution of Poisson equation:

$$\Delta z = f \quad \Leftrightarrow \quad z(x) = \aleph_N * f(x) = \int_{R^N} \aleph_N(x - y) f(y)\, dy \quad \text{with } \aleph_N(x) = \begin{cases} (2\pi)^{-1} \ln|x| & \text{if } N = 2 \\ ((2 - N)\sigma_N)^{-1} |x|^{2-N} & \text{if } N = 3 \end{cases} \tag{1}$$

Then, we are able to write pressure in an integral form:

$$p(t,x) = \int_{R^N} \aleph_N(x-y)\,\mathrm{tr}\big(\nabla u(t,y)\big)^2\,\mathrm{d}y \tag{2}$$

and we can deduce pressure gradient:

$$\nabla p(t,x) = \nabla \aleph_N * \mathrm{tr}(\nabla u)^2(x) = C_N \int_{R^N} \frac{x-y}{|x-y|^N}\,\mathrm{tr}\big(\nabla u(t,y)\big)^2\,\mathrm{d}y \tag{3}$$

The last term allows to delete pressure term in the Navier equation:

$$D_t u(t,x) = \nu\Delta u - C_N \int_{R^N} \frac{x-y}{|x-y|^N}\,\mathrm{tr}\big(\nabla u(t,y)\big)^2\,\mathrm{d}y \tag{4}$$

This last equation drives speed evolution of wake vortices, but cannot be easily exploited to roll-up kinematic characterization. Alternatively, tangential speed in roll-up will be modeled by empirical laws. Classically, velocity profile (tangential speed at radius r) is defined by:

$$v_\theta(r) = \frac{\Gamma_0}{2\pi r}\big(1 - e^{-f(\frac{r}{B})}\big)$$

where Γ_0 is called circulation, that can be deduced by the following mechanical equalities. When the forces which act on the aircraft are in balance, the aircraft lift and the flux of wake vertical momentum are also equal to the weight of the aircraft. We can then observe that wake vortex circulation strength (root circulation in m^2/s) is proportional to aircraft mass and inversely proportional to wingspan and aircraft speed [6]:

$$\Gamma_0 = \frac{Mg}{(\rho V s B)} \begin{cases} M\text{: aircraft mass} \\ V\text{: aircraft speed} \\ B\text{: wingspan} \end{cases} \begin{cases} g\text{: gravitational acceleration} \\ \rho\text{: air density} \\ \Gamma_0\text{: root circulation} \\ s = \pi/4 \end{cases} \tag{5}$$

For a single and axi-symmetric vortex the circulation is given by: $\Gamma(r) = 2\pi r v_\theta(r)$.

Other characteristics of wake vortices are given by:

- Initial vortex spacing (m):

$$b_0 = sB \quad \text{with } s = \frac{\pi}{4} \tag{6}$$

- The two counter rotating vortices rolling off the wing tips create a downwash velocity that pulls the wake vortex pair down after leaving the aircraft. Descent speed of vortex pairs (m/s):

$$\frac{\Gamma_0}{2\pi b_0} \tag{7}$$

Additional factors that induced specific dynamic of wake vortices, illustrated in Fig. 1, are: Wind Shear Effect (stratification of wind), Ground Effect (rebound), Transport by Cross-wind & Decay by atmospheric turbulence and Crow instability.

The next value, we need to know, is the characteristic time scale for the wake vortex to decay. The two counter rotating vortices rolling off the wing tips create a downwash velocity that pulls the wake vortex pair down after leaving the aircraft. A characteristic time scale can be defined as the time it takes for the vortex pairs to descend one wing span (t'). Time taken for the vortex pairs to descend one wing span: $t' = 0.38\frac{B^3 V}{M}$. If the ambient background turbulence eddy dissipation rate [19–22] ε is measured to be above a threshold value, $\varepsilon \geqslant 10^{-4}\ \mathrm{m}^2/\mathrm{s}^2$, the crow instability is empirically observed to lead to a coherent circulation decay rate.

Once this background threshold is exceeded, the accelerated wake vortex circulation decay rate can be bound by the empirical observed equation and is predicted to be bellow naturally occurring atmospheric turbulent levels near the ground in 8 to 9 non-dimensional time periods:

$$\Gamma = \Gamma_0\left(1 - \frac{t^*}{8}\right) \quad \text{with } t^* = \frac{t}{t'} \tag{8}$$

It is reasonable for a conservative safe separation distance to be determined by the time it takes for the preceding aircraft's wake to decay to an observed typical atmospheric boundary layer background circulation level of $\Gamma_{bg} = 70\ \mathrm{m}^2/\mathrm{s}$.

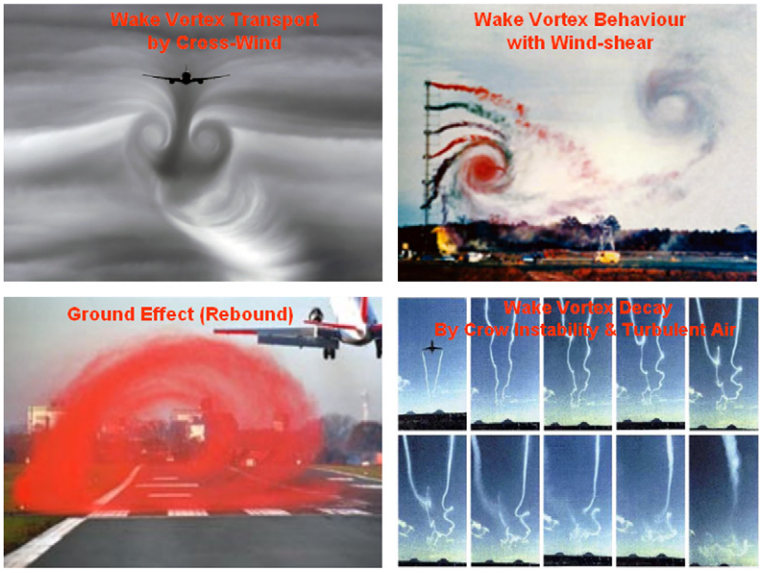

Fig. 1. Wake vortex dynamics and behavior.

Then, we obtain by using preceding equations:

$$t_{\Gamma_{bg}} = 8t'\left(1 - \frac{\Gamma_{bg}}{\Gamma_0}\right) \tag{9}$$

3. Theoretical model of wake vortex radar cross section

Up to now, there was much research on wake vortex detection with radar on different frequency bands [5,7–9,13–18, 20,23–26]. To collect data in different weather conditions, the X-band Radar BOR-A 550 was deployed at Paris-CDG Airport, co-localized with 2 μm Lidar from Eurocontrol, to monitor runways during take-off and landing. In these scenarios, Radar measurements on different weather conditions were performed for benchmarking technology with Lidar one.

During the 1980s and 1990s different radar trials have been made in UK, France & US for wake vortex monitoring in clear air with positive results for different bands (VHF/UHF/L/S/C/X bands) at short range (few kilometers). US radar campaigns are detailed by Gilson [17,18] and Shariff and Wray in [15].

In Europe, joint radar trials have been made:

- *Sheppard* [7]: detection at range $R = 2.8$ km with an S-band Radar (3 GHz) (DX 04 Radar Campaign by GEC-MARCONI);
- *Bertin* [8,9]: detection at range $R = 0.5$ km with a UHF-band Radar (961 MHz) (PROUST Radar campaign by CNRS/CRPE).

In Gilson [17,18], it was observed that wake vortex RCS was relatively flat as a function of frequency. Particulates were not involved (they would give f^4 Rayleigh scattering). The frequency dependence was not the Kolmogorov $f^{1/3}$. Furthermore, the RCS measurement 1 km behind the plane was insensitive to engine thrust and flat setting.

In [16], tests have revealed radar echoes from aircraft wakes in clear air. The mechanism causing refractive index gradients in these tests is thought to be the same as that for homogeneous and isotropic atmospheric turbulence in the Kolmogorov inertial range, for which there is a scattering analysis due to Tatarski [4]: in a turbulent velocity field the presence of mean vertical gradients of potential temperature and humidity lead to fluctuations in refractive index (the radar cross section per unit volume of isotropic turbulence in the inertial range is $\eta = 0.38C_n^2\lambda^{-1/3}$). Mechanism does not depend on atmospheric conditions (humidity has a weak influence) and Engine Exhaust has no role.

Two main mechanisms causing refractive index gradients have been considered [16]:

- **Radial density gradient in the vortex cores:** The core of each vortex, which has a lower density and therefore lower index of refraction. Radial pressure (and therefore density) gradient in a columnar vortex arising from the rotational flow. The RCS is due to a density gradient in a vortex arising from a balance of radial pressure gradient and centrifugal forces:

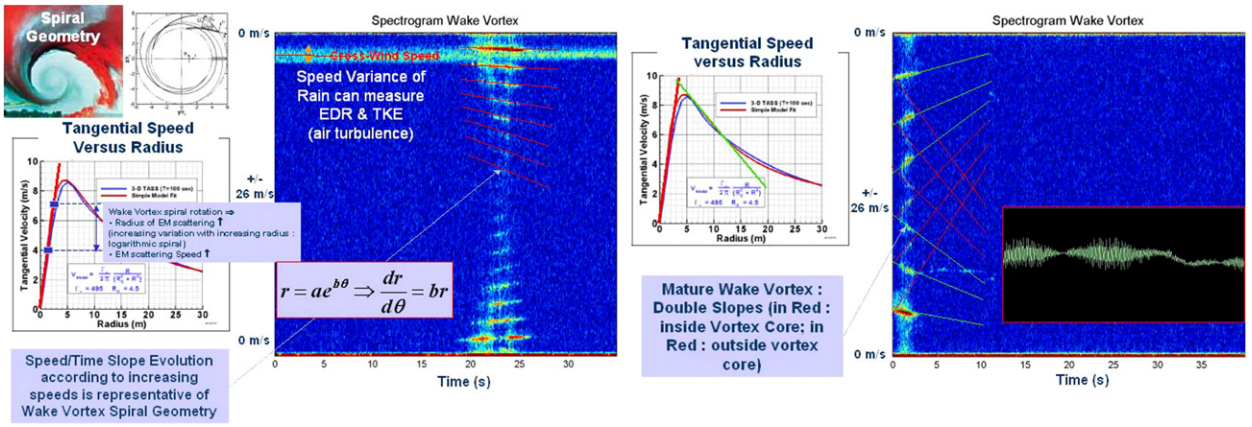

Fig. 2. Time/speed slope evolution representative of wake vortex (logarithmic) spiral geometry.

$$(n-1)\times 10^6 = 77.6\left(\frac{P_a}{T}\right) + 64.8\left(\frac{P_v}{T}\right) + 3.776\times 10^5\left(\frac{P_v}{T^2}\right)$$

$$\text{with}\begin{cases} n\text{: refractive index of humid air for frequ. below 20 GHz} \\ P_a\text{: the partial pressure (mb) of dry air} \\ P_v\text{: the partial pressure (mb) of water vapour} \\ T\text{: the temperature (K), } T_\infty = 288\text{ K} \end{cases}$$

$$\frac{P(r)}{P_\infty} = \left(\frac{\rho(r)}{\rho_\infty}\right)^\gamma = \left(1-(\gamma-1)\int_r^\infty \frac{1}{r}\frac{V_\theta^2}{c_\infty^2}\,\mathrm{d}r\right)^{\gamma/(\gamma-1)}$$

$$\text{with } V_\theta = \frac{\Gamma}{2\pi r}\begin{cases} (r^2/r_0^2) & \text{for } r < r_0 \\ 1 & \text{for } r \geqslant r_0 \end{cases} \quad \text{where} \begin{cases} \rho(r)\text{: density in each vortex} \\ \rho_\infty\text{: ambient density} \\ c_\infty\text{: the ambient speed of sound (341 m/s)} \end{cases}$$

$$\text{and}\quad \frac{T(r)}{T_\infty} = \left(\frac{P(r)}{P_\infty}\right)\left(\frac{\rho(r)}{\rho_\infty}\right)^{-1} \tag{10}$$

- **Transport of atmospheric fluid in the oval surrounding the vortices:** The oval surrounding the vortex pair that transports atmospheric air from one altitude to another. As it descends, the fluid in the oval compresses adiabatically in response to increasing ambient pressure.

$$\left[\tilde{n}(z)-\bar{n}(z)\right]\times 10^6 = 223\left[\tilde{\rho}(z)-\bar{\rho}(z)\right] + 76.7\left[\tilde{\rho}_v(z)-\bar{\rho}_v(z)\right] + 1.75\times 10^6\left[\frac{\tilde{\rho}_v(z)}{\tilde{T}(z)} - \frac{\bar{\rho}_v}{\bar{T}(z)}(z)\right]$$

$$\left[\tilde{n}(z)-\bar{n}(z)\right]\times 10^6 = -\frac{\bar{\rho}(z)N^2}{g}\Delta z\left[223 + \frac{\overline{RH}(z)P_{sat}(T_z)}{\bar{P}(z)}\left(76.7 + \frac{3.49\times 10^6}{\bar{T}(z)}\right)\right]$$

$$\text{with}\begin{cases} N\text{: Brünt–Väisälä frequency} \\ \text{at sea level: } N = 0.014s^{-1}\text{ (in summer)} \\ N = 0.02s^{-1}\text{–}0.03s^{-1}\text{ (in winter)} \\ \Delta z\text{: descend altitude} \\ P = P_a + P_v \end{cases} \tag{11}$$

- **Other potential causes of wake vortex reflectivity:** There is another mechanism which could generate an echo, it is the collective distribution [43]. This mechanism does not require discontinuities but only spatial fluctuations in the index. Spatial Fourier Transform of the optical index field characterizes the fluctuations. The fluctuations which provide the echo are the ones which correspond to a vector of wave $\bar{k}$ of opposite steering to the vector of incident wave $\bar{k}_0$ and its number of wave is double: $\bar{k} = -2\bar{k}_0$. The turbulence generated by the vortex extends in all the scales up to the dissipation scale. The fluctuations scale which provides the collective distribution is 1.5 cm, a value very superior on the diffusion scale. So a part of the radar echo can be generate by the collective distribution. This effect increases the detectability of the vortex, but it can also change the interpretation of the successful signal, because then an echo can come even if there is no layer of discontinuity normal for the radar line of sight.

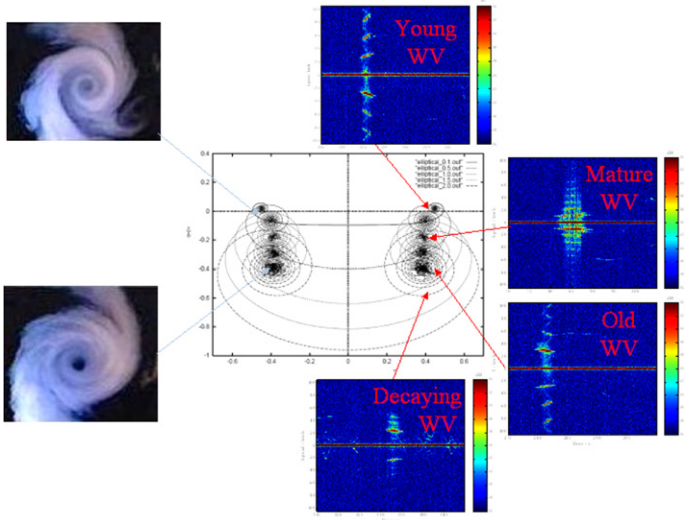

Fig. 3. Evolution of roll-up spiral geometry & Doppler spectrum (time/Doppler slopes) versus age.

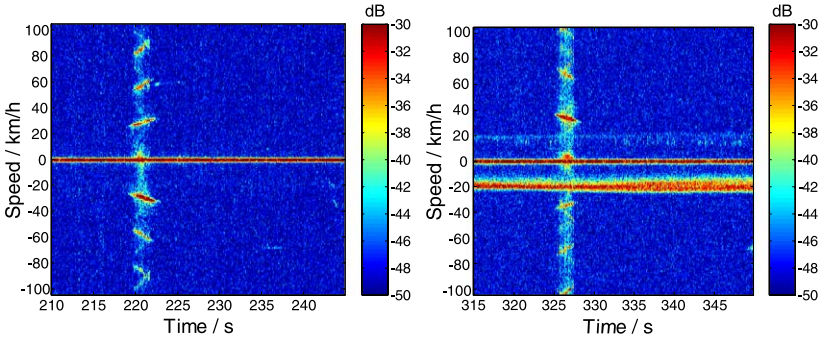

Fig. 4. Time/speed slope evolution representative of wake in clear air (left) and in rain (right).

4. X-band Doppler radar signature of a wake vortex

The data-recording unit stores the complex radar video signal with a range gate size of 40 m. This allows the recording of 5 range cells (200 m range swath) using a peak pulse power of 20 Watts (75 Watts in the new version). With the applied PRF, a Doppler velocity resolution of 0.2 m/s is achieved.

We observe, on the time/Doppler signature, slopes in time/Doppler(speed) that can be interpreted by logarithmic spiral structure of wake vortex. Roll-ups are interlacing fences of air from surrounding and from higher altitude (adiabatic transport of fluid within vortex pair). When each roll-up rotates, range of reflecting points at each fence increase. According to wake vortex age and tangential speed law, this range evolution induced positive time/Doppler slopes (young vortex), jointly positive/negative slopes (mature vortex), negative slopes (old & decaying vortices). In Fig. 3, spiral geometry of contra-rotating vortex roll-ups is illustrated. We can observe that roll-up curvature evolves with radius and time. For a “young vortex”, wake core is dense with high tangential speed increasing with radius. On the contrary for an “old vortex”, their cores have been destroyed by diffusion and tangential speed decrease with radius.

Time/speed spectra (Figs. 1 to 7), deduced from time/Doppler frequency spectrum, show systematically the presence of multiple speeds in integer ratios between them. We can understand the simultaneous presence in the radar cell of multiple speeds by vortex spiral geometry and intermittent reflectivity of successive fences and they should not be interpreted by harmonics.

In staring mode the direction of the antenna beam is fixed with a beam width of 2.7°. It was directed towards a point below the starting path after take-off. Fig. 4 shows the Doppler signature of a wake vortex in two different kind of weather conditions: clear air and rainy weather. We can observe that we have the same signature for wet and dry air and same kind of reflectivity.

Fig. 5 (left) contains the Doppler signature of a mature wake vortex. The radial speed remains almost constant over time. Moreover, Fig. 5 (middle) shows a recording of a wake vortex, which has started to decay, and Fig. 5 (right) presents the spectrogram of an almost decayed vortex.

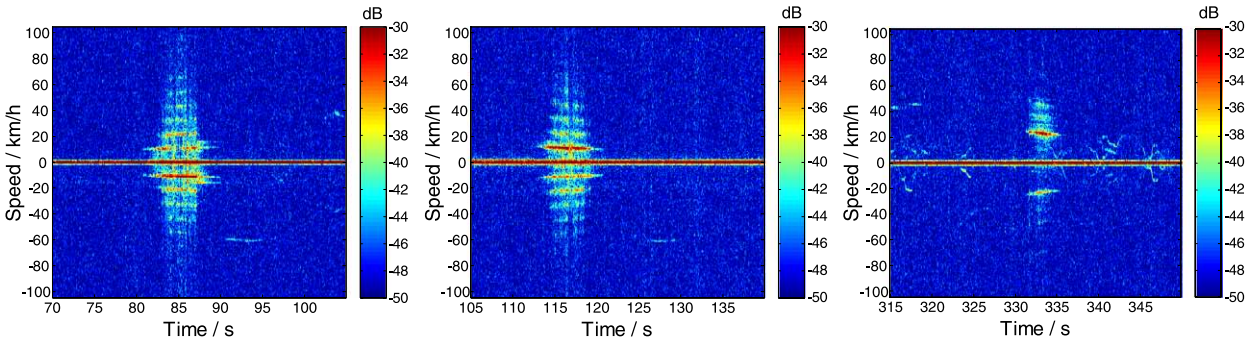

Fig. 5. Doppler signature of a mature wake vortex (left), a decaying wake vortex (middle), and a decayed wake vortex (right).

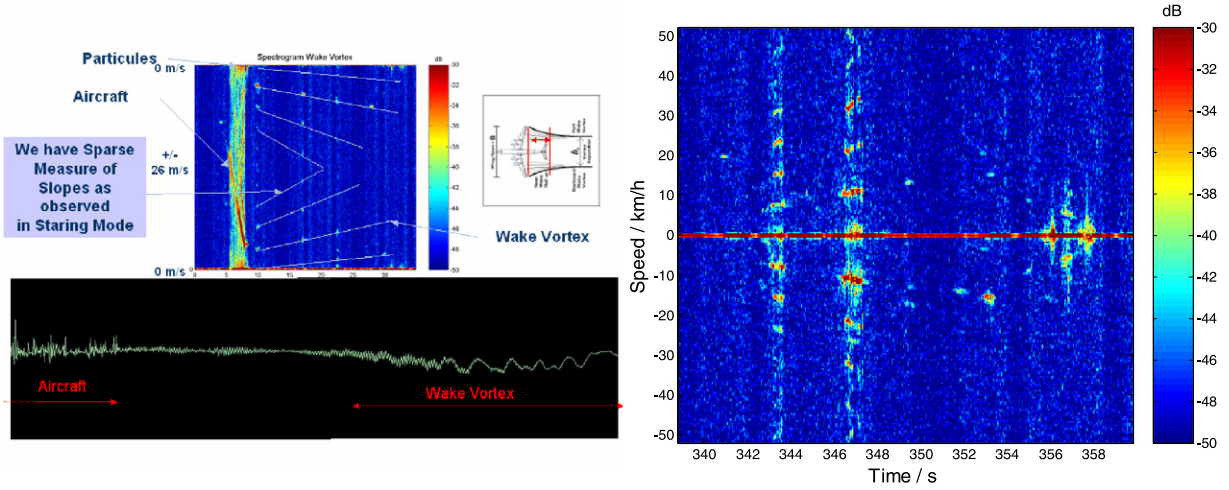

Fig. 6. Doppler signature in scanning mode.

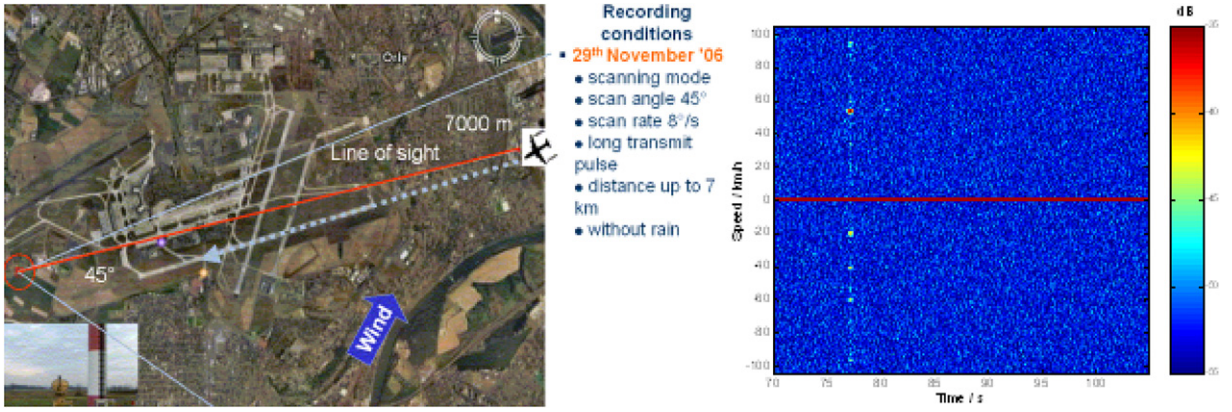

Fig. 7. Wake vortex monitoring at 7 km range.

In scanning mode (Fig. 6) the radar was continuously scanning a surveillance area of 45° with a speed of about 8°/s. In this area, wake vortices of medium sized (B737 & A320) planes have been all detected. For more heavy aircrafts (A380 & B747-8), performances could be drastically improved. Due to the scanning process a number of sparse samples of the vortices are visible. Nevertheless, the speed components of the wake vortex can be tracked from scan to scan. Analysis of data obtained in scanning mode gives the same kind of information, than in staring, on the wake vortex geometry and age.

The data recordings described above covered a range from 500 to 700 m. With the signal format used in this case a detection range up to 1000 m for wake vortex encounters can be assumed. At the end of the Orly trial the area beneath the glide path for landing planes was monitored in scan mode. In that case a longer pulse was used. Anecdotally, some very short wake vortex detections were also obtained at a distance of 7000 m using a sector width of 45°. In Fig. 7, the

spectrogram of a sample of the recorded data is illustrated. It should be noted that in this case the landing path was in parallel to the radar beam, causing a receiving position that was clearly far from optimal. The distance and the angle caused a very low detection probability, but still some traces of wake vortex encounters could be found. Wake vortex detection range of 1/2 km is compliant with operational request related to monitoring along the runway and glide slope.

5. Advanced Doppler processing chain for wake vortex monitoring

Based on recording of Doppler complex I & Q data, an advanced processing chain has been developed to:

- ***Detect wake vortex*** (in wet & dry conditions) at short range (<1.5 km) in scanning mode (8°/s);
- ***Localize wake vortex*** in range/azimuth;
- ***Characterize wake vortex:*** geometry (roll-up spiral), age & strength (circulation in m^2/s).

Wake vortex detection is based on Regularized High Resolution Doppler analysis. For this function, we have developed and tested a highly sensitive detector based on High Resolution Doppler entropy assessment. First, radar cells are localized by a threshold on Doppler entropy, that is defined by means of information geometry [36–38]:

$$S = \sum_{k=2}^{n-1} (n-k)\left(\frac{1}{2}\ln\left(\frac{1+|\mu_k|}{1-|\mu_k|}\right)\right)^2$$

with $\{\mu_k\}_{k=2,\ldots,n-1}$ reflection coefficient of complex regularized Autoregressive model.

From I & Q data, $x(k)$, $k=1,\ldots,N$ (N number of pulses in one burst) and a Lagrangian parameter for regularization γ_1, a regularized complex autoregressive model is computed at maximum order $M=N-1$. From autoregressive parameters $a_k^{(M)}$, $k=0,\ldots,M$. Regularized Burg reflection coefficients μ_k, $k=1,\ldots,M$ are computed (P_M is power of autoregressive estimation error). Regularized Burg Algorithm is given by:

Initialization:

$$f_0(k) = b_0(k) = x(k), \quad k=1,\ldots,N \ (N\text{: n.b. samples})$$

$$P_0 = \frac{1}{N}\sum_{k=1}^{N}\left|x(k)\right|^2, \quad a_0^{(0)} = 1$$

Iteration (n): for $n=1$ to M:

$$\mu_n = -\frac{\frac{2}{N-n}\sum_{k=n+1}^{N} f_{n-1}(k)b_{n-1}^*(k-1) + 2\sum_{k=1}^{n-1}\beta_k^{(n)}a_k^{(n-1)}a_{n-k}^{(n-1)}}{\frac{1}{N-n}\sum_{k=n+1}^{N}|f_{n-1}(k)|^2 + |b_{n-1}(k-1)|^2 + 2\sum_{k=0}^{n-1}\beta_k^{(n)}|a_k^{(n-1)}|^2} \quad \text{with } \beta_k^{(n)} = \gamma_1(2\pi)^2(k-n)^2$$

$$\begin{cases} a_0^{(n)} = 1 \\ a_k^{(n)} = a_k^{(n-1)} + \mu_n a_{n-k}^{(n-1)*}, \quad k=1,\ldots,n-1, \\ a_n^{(n)} = \mu_n \end{cases} \quad \text{and} \quad \begin{cases} f_n(k) = f_{n-1}(k) + \mu_n b_{n-1}(k-1) \\ b_n(k) = b_{n-1}(k-1) + \mu_n^* f_{n-1}(k) \end{cases} \tag{12}$$

For each cell that has been detected with potential hazard, wake vortex strength is deduced [10–12] from circulation computed from $S(V_i)$ the spectral magnitude of a Doppler velocity bin, after previously applying CFAR on Doppler axis to extract Doppler peaks in spectrum:

$$\Gamma \propto \left[2\int_{V_{\min}}^{V_{\max}} V_i^2\left[S(V_i)\right]^{2/3}\mathrm{d}V_i\right] \Big/ \left[\int_{V_{\min}}^{V_{\max}}\left[S(V_i)\right]^{2/3}\mathrm{d}V_i\right] \tag{13}$$

Empirical law of tangential speed parameterized by vortex radius r is given by:

$$V_r = \begin{cases} \frac{r}{r_c}V_{\max} & \text{if } 0 \leqslant |r| \leqslant r_c \\ \frac{r_c}{r}V_{\max} & \text{if } r_c \leqslant |r| \end{cases} \tag{14}$$

Doppler spectrum is generated by speed in the roll-up:

$$S(V_i) = \int_{-\pi/2}^{+\pi/2}\int_{r(v_i)}^{r(V_i+\Delta V)} V_i\,\mathrm{d}\theta\,r\,\mathrm{d}r = \int_{-\pi/2}^{+\pi/2}\int_{r(v_i)}^{r(V_i+\Delta V)} V_r\cos\theta\,\mathrm{d}\theta\,r\,\mathrm{d}r \tag{15}$$

Circulation, defined by the following integral, can be developed with speed empirical law:

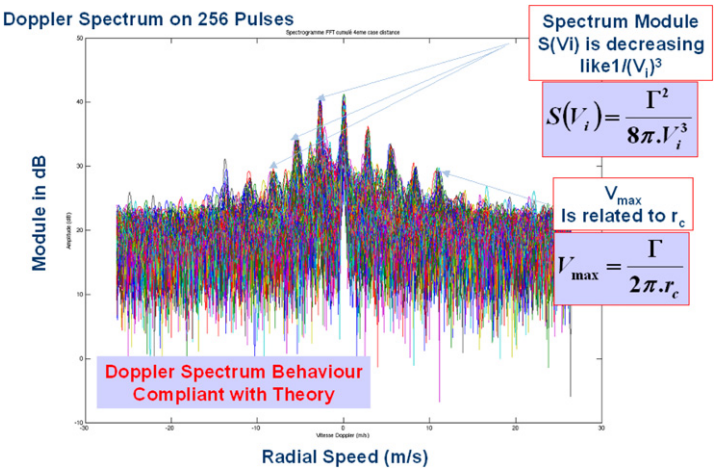

Fig. 8. Doppler FFT for all radar cells in case of wake vortex.

$$\Gamma(r)=\int_0^{2\pi} rV_r\,\mathrm{d}\theta=\int_0^{2\pi} r\frac{r_c}{r}V_{\max}\,\mathrm{d}\theta=2\pi r_c V_{\max}=\Gamma$$

$$\Rightarrow\quad V_{\max}=\frac{\Gamma}{2\pi r_c}\quad\text{and}\quad V_r=\frac{r_c}{r}V_{\max}=\frac{\Gamma}{2\pi r}\quad\text{if } r_c\leqslant|r| \tag{16}$$

Considering the Doppler speed:

$$V_i=V_r\cos\theta=\frac{\Gamma\cos\theta}{2\pi r}\quad\Rightarrow\quad S(V_i)=\frac{\Gamma}{\pi}\int_{-\pi/2}^{+\pi/2}\int_{r(V_i)}^{r(V_I+\Delta V)}\cos\theta\,\mathrm{d}\theta\,\mathrm{d}r=\int_{-\pi/2}^{+\pi/2}\int_0^{\cos\theta\frac{\Gamma}{2\pi V_i}} r\,\mathrm{d}r \tag{17}$$

The area for $V>V_I$, is given by:

$$A=\int_{-\pi/2}^{+\pi/2}\mathrm{d}\theta\int_0^{r(V_I)} r\,\mathrm{d}r=\int_{-\pi/2}^{+\pi/2}\mathrm{d}\theta\int_0^{\cos\theta\frac{\Gamma}{2\pi V_i}} r\,\mathrm{d}r=\int_{-\pi/2}^{+\pi/2}\left[\frac{r^2}{2}\right]_0^{\cos\theta\frac{\Gamma}{2\pi V_i}}\mathrm{d}\theta=\frac{1}{2}\left(\frac{\Gamma}{2\pi V_i}\right)^2\int_{-\pi/2}^{+\pi/2}\cos^2\theta\,\mathrm{d}\theta=\frac{\Gamma^2}{16\pi V_i^2} \tag{18}$$

This derivative of previous area is related to Doppler spectrum by

$$S(V_i)=\frac{\mathrm{d}A}{\mathrm{d}V_i}=\frac{\Gamma^2}{8\pi V_i^3} \tag{19}$$

Then, we can compute the following normalized moment (Fig. 8):

$$2\frac{\int_{V_{\min}}^{V_{\max}} V_i^2[S(V_i)]^{2/3}\,\mathrm{d}V_I}{\int_{V_{\min}}^{V_{\max}}[S(V_i)]^{2/3}\,\mathrm{d}V_i}=k_1\frac{\int_{V_{\min}}^{V_{\max}}\mathrm{d}V_i}{\int_{V_{\min}}^{V_{\max}}\frac{1}{V_i^2}\,\mathrm{d}V_i}=k_1V_{\max}V_{\min}=k_2V_{\max} \tag{20}$$

with $k_1=2$ and $k_2=k_1V_{\min}$. By identifying with second expression of circulation $\Gamma=2\pi r_cV_{\max}$, we can recover Rubin expression [10–12] for Circulation assessment:

$$\Gamma=k_3\cdot 2\frac{\int_{V_{\min}}^{V_{\max}} V_i^2[S(V_i)]^{2/3}\,\mathrm{d}V_I}{\int_{V_{\min}}^{V_{\max}}[S(V_i)]^{2/3}\,\mathrm{d}V_i}\quad\text{with } k_3=\frac{2\pi r_c}{k_2} \tag{21}$$

Information on wake vortex roll-up spiral geometry is given by $r=ae^{b\theta}\Rightarrow\frac{\mathrm{d}r}{\mathrm{d}\theta}=br$ where parameter "b" is deduced from time/Doppler spectrum evolution:

$$\begin{cases}V(r)=\frac{\Gamma_0}{2\pi r_c}\frac{r}{r_c}\\ r=ae^{b\theta}\end{cases}\quad\Rightarrow\quad b=\frac{1}{2\pi}\log\left(1+\frac{\delta_rV}{V}\right) \tag{22}$$

This equation is deduced from spiral model:

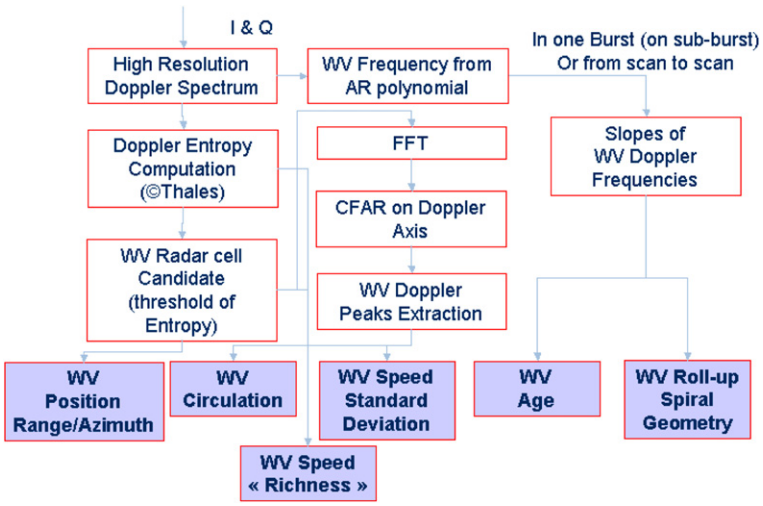

Fig. 9. Doppler radar processing chain for wake vortex monitoring.

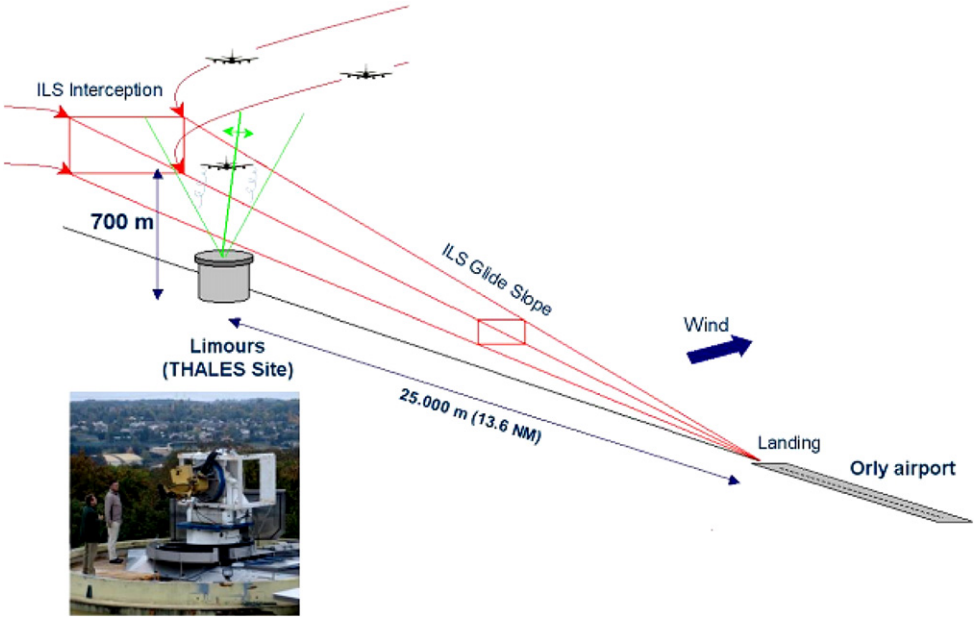

Fig. 10. Description of radar trials at Thales Limours premises for wake vortex monitoring in Orly glide slope.

$$\begin{cases} V(r) = \frac{\Gamma_0}{2\pi r_c}\frac{r}{r_c} \quad \Rightarrow \quad V(r) = \alpha r \\ r = ae^{b\theta} \quad \Rightarrow \quad r + \delta r = ae^{b(\theta+2\pi)} = re^{b2\pi} \quad \Rightarrow \quad \frac{r+\delta r}{r} = e^{b2\pi} \quad \Rightarrow \quad \frac{\delta r}{r} = e^{b2\pi} - 1 \\ V = \alpha r \quad \Rightarrow \quad \frac{\delta_r V}{V} = \frac{\delta r}{r} = e^{b2\pi} - 1 \quad \Rightarrow \quad b = \frac{1}{2\pi}\log(1 + \frac{\delta_r V}{V}) \end{cases} \tag{23}$$

In Fig. 9, we illustrate global processing chain for wake vortex detection, circulation assessment and roll-up spiral geometry profiling.

6. Paris Orly and Paris-CDG Airport campaigns

Before deployment at CDG Airport, some tests have been made in Orly by monitoring wake vortex in the glide slope of arrivals. During these first tests, wake vortex at altitude of 1500 m has been clearly detected and tracked from scan to scan in very turbulent atmosphere (capacity that is not available by Lidar). Radar was operated with a vertical scanning mode at 8°/s. Trial test plans are given in Figs. 10 and 11.

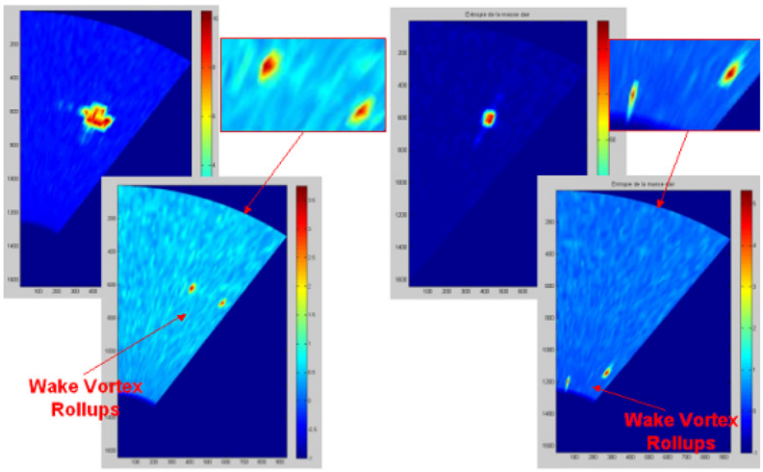

Fig. 11. Monitoring of clear air wake vortex monitoring at range 1500 m based on high resolution Doppler.

Fig. 12. X-band Radar deployment at Paris-CDG Airport, co-localized with 2-micron Eurocontrol Lidar, in horizontal & vertical scanning modes.

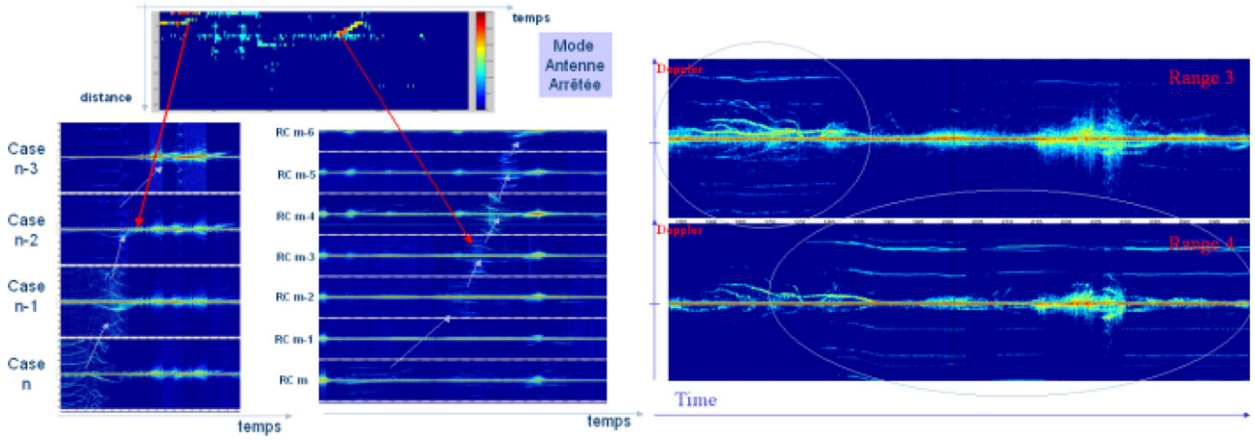

Fig. 13. Wake vortex time/Doppler spectrum from range to range (at left) and in range cell 3 & 4 (at right).

Finally, in June 2008, BOR-A radar has been deployed at Paris-CDG Airport, and co-localized with a 2-micron Lidar from Eurocontrol. Radar has been operated in vertical and horizontal scanning modes, to monitor arrivals and departures along south closely spaced parallel runways, as illustrated in Fig. 12.

In a first step, antenna was used in a staring mode for vertical exploration by exploitation of 4° beamwidth. In the following figure, we illustrate wake vortex detection by Doppler entropy in time/range coordinate axes. After each departure on the first nearer runways, wake vortexes were monitored.

As soon as a radar cell has revealed presence of wake vortex by its radar entropy, wake vortex circulation is computed as illustrated in Fig. 9.

The Doppler spectra with the wake vortex are characteristic of the vortex roll-up geometry as illustrated in Fig. 13.

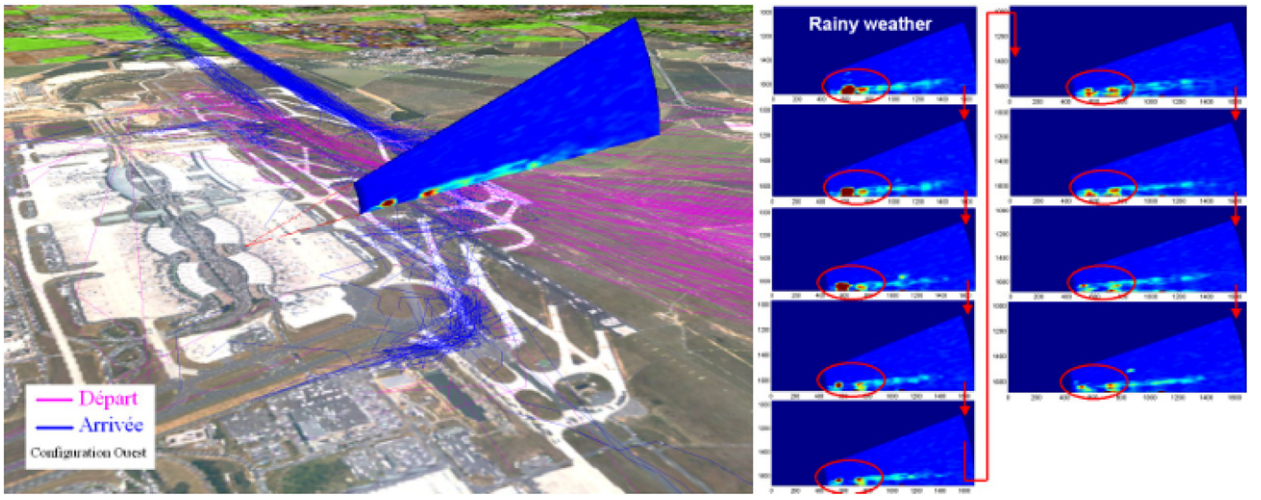

Fig. 14. Wake vortex roll-ups tracking from scan to scan in rainy weather.

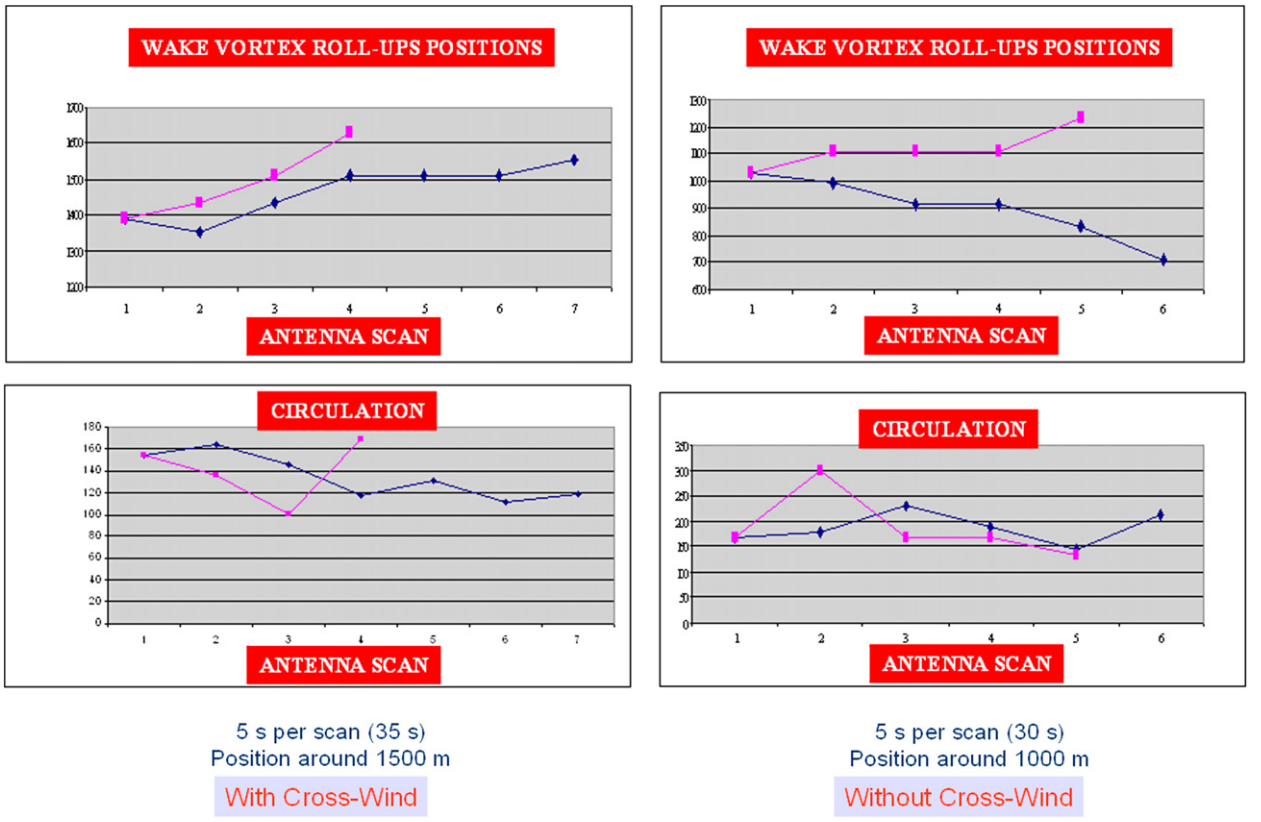

Fig. 15. Wake vortex position & circulation (strength in m^2/s) along runway with cross-wind on the left and without cross-wind on the right.

In vertical scanning mode, we were able to track individual roll-up of each wake vortex in range and elevation axes. In Fig. 14, we can observe, above the first nearer runway, wake vortex generated by aircraft during departure. These detections of wake vortex are coherent with classical behavior close to the ground.

Wake vortexes generated by aircraft during departure on the first runway are illustrated. We prove that we can track each roll-up from scan to scan (with one scan every 5 seconds). Close to the ground, we can finely follow trajectory of each roll-up and estimate their strength by circulation computation.

Based on these elementary detections, results have been exploited and synthesized to benchmark Lidar and Radar technologies. This task of benchmarching will be done by Eurocontrol Bretigny Experimental Center. In Fig. 15, we give positions

and circulations of each wake vortex roll-up (right and left) for the first 30 s, every 5 s. This case illustrates weather conditions with and without cross-wind.

7. Conclusion

X-band radar has proved some capabilities to monitor wake vortex for different weather conditions (light to heavy rain, fog, turbulent atmosphere, etc.) with a fast monitoring of very large volume (radar scanning) with high update rate (8°/s with mechanical scanning for BOR-A radar). In these first experiments, radar seems to have higher sensitivity than Lidar sensor, like capability for monitoring of "medium" aircrafts wake vortex (most common aircraft at CDG, e.g. A320) and not only "heavy/super heavy", that is needed for traffic mix of "very light jets". With low cost electronic scanning antenna, these radar capabilities could be improved [35].

This capability could be exploited for operational use to track wake vortex (transport, decay, rebound) in extreme weather conditions: wind burst (wind under storm, turbulent atmosphere, wind shear, etc.), no wind (foggy weather, etc.). This capability could be also helpful for non-operational use like "Safety Case" by data collection: risks assessment according to extreme wind conditions and not on average wind conditions, need for wake vortex data collection in exhaustive cases of airport climatology (good/bad weather).

References

[1] Jean-Yves Chemin, Jean Leray et les fondements mathématiques de la turbulence, coll. Un texte un mathématicien, Société Mathématique de France, 14 février 2007.
[2] Jean-Yves Chemin, Le système de Navier–Stokes incompressible, soixante dix-ans après Jean Leray, in: Séminaires et Congrès, vol. 9, Société Mathématique de France, 2004, pp. 99–123.
[3] Yves Meyer, Jean Leray et la recherche de la vérité, Journées anniversaire Jean Leray, Nantes.
[4] V.I. Tatarski, Wave Propagation in a Turbulent Medium, McGraw-Hill, 1661.
[5] D.C. Burnham, Review of wake vortex sensor development since 1970, in: Proceedings of the Aircraft Wake Vortices Conference, Report No. FAA-RD-77-68, June 1977.
[6] F. Holzälpfel, et al., Analysis of wake vortex decay mechanisms in the atmosphere, Aerospace Science & Technology 7 (2003) 263–275.
[7] D.J. Shephard, A.P. Kyte, P.D.F. Tait, Radar measurement of the wake vortex of a H.S. 748 and a B.A.C. one-eleven, Preliminary trials report, MTR-92/55A, GEC-Marconi Research Center, 1992.
[8] T. Tani, F. Bertin, Restitution en temps réel du champ de vitesses créé par des vortex d'avions, Convention d'étude CNRS/CRPE & STNA, 1992.
[9] G. Rat, F. Bertin, Etude théorique de la détection des vortex générés dans le sillage des avions à l'aide d'un radar, CNRS/CRPE, 1992.
[10] William L. Rubin, Radar–acoustic detection of aircraft wake vortices, Journal of Atmospheric and Oceanic Technology 17 (8) (August 2000) 1058–1065.
[11] William L. Rubin, Detection and strength measurement of wake vortices at JFK using RASS, Final report, WLR Research Inc., Whitestone, NY, FAA Contract DTFAO1-92C-00061.
[12] W.L. Rubin, D.C. Burnham, E.A. Spitzer, R.P. Rudis, Robust low cost airport wake vortex sensor, Journal of Aircraft 37 (3) (2000) 377–382.
[13] P.J. Morris, D.K. McLaughlin, T.B. Gabrielson, The development of a plan for the assessment, improvement and deployment of a Radar Acoustic Sounding System (RASS) for wake vortex detection (Final report), NASA Grant NAG1-03084, NASA Langley Research Center, September 2004.
[14] S. Boluriaan, P.J. Morris, Two-dimensional simulations of wake vortex detection using RASS, AIAA Journal 40 (11) (2002) 224–2256.
[15] K. Shariff, Analysis of the radar reflectivity of aircraft vortex wakes, Journal of Fluid Mechanics 463 (2002) 121–161.
[16] K. Chadwick, et al., Radar cross section measurements of a wingtip vortices, in: Proc. ESA IGARSS, vol. 1, 1984, pp. 479–483.
[17] W.H. Gilson, Radar measurements of aircraft wakes, Project Rep. AAW-11, Lincoln Lab, MIT, Lexington, Mass, 1992.
[18] W.H. Gilson, Aircraft RCS measurement, in: NASA Contractor Rep. 10139, Part 2, 1994, pp. 603–623.
[19] S.A. Cohn, Radar Measurements of Turbulent Eddy Dissipation Rate in the Troposphere: A Comparison of Techniques, American Meteorological Society, 1995.
[20] W.K. Hocking, Measurement of turbulent eddy dissipation rates in the middle atmosphere by radar techniques: A review, Radio Science 20 (1985) 1403–1422.
[21] E.E. Gossard, R.G. Strauch, Radar Observations of Clear Air and Clouds, Elsevier, 1983.
[22] A.S. Frisch, R.G. Strauch, Doppler radar measurements of turbulent kinetic energy dissipation rates in a northeastern Colorado convective storm, Journal of Applied Meteorology 15 (1976) 1012–1017.
[23] P. Iannuzelli, et al., Aircraft wake detection using bistatic radar: analysis of experimental results, John Hopkins Appl. Phys. Lab. Tech. Digest 19 (1998) 299–314.
[24] R.E. Marshall, T.J. Myers, Wingtip generated wake vortices as radar targets, IEEE AES Systems Magazine (1996) 27–30.
[25] R. Nespor, et al., Doppler radar detection of vortex hazard indicators, in: NASA Conf. Proc. CP-10139, Part 2, 1994, pp. 651–688.
[26] H. Otterstein, Atmospheric structure and radar backscattering in clear air, Radio Science 4 (1969) 1179–1193.
[27] F. Barbaresco, U. Meier, Wake vortex data collection using X-band radar, in: CEAS'07, Berlin, 2007.
[28] F. Barbaresco, U. Meier, Wake vortex detection & monitoring by X-band radar, in: Radar Conference, Edinburgh, 2007.
[29] F. Barbaresco, et al., Wake vortex monitoring & profiling by Doppler X-band radar in all weather conditions, in: 6th Eurocontrol Innovation Workshop, France, December 2007.
[30] F. Barbaresco, U. Meier, Wake vortex profiling by Doppler X-band radar: Orly trials at initial take-off & ILS interception critical areas, in: IEEE Int. Radar Conf., RadarCon'08, Rome, May 2008.
[31] F. Barbaresco, U. Meier, Study of wake vortex roll up spiral geometry based on radar trials, in: Int. Workshop on Fundamental Issues Related to Aircraft Trailing Wakes, Marseille, May 2008.
[32] F. Barbaresco, U. Meier, Wake vortex X-band radar monitoring: Paris-CDG airport 2008 campaign results & perspectives, in: Wakenet3—Europe Workshop on "Wake Turbulence Safety in Future Aircraft Operations", Thales University, Jouy-en-Josas, Janvier 2009.
[33] F. Barbaresco, U. Meier, Paris-CDG airport trials for wake vortex X-band monitoring, in: International Radar Symposium, IRS'09, Hamburg, September 2009.
[34] F. Barbaresco, U. Meier, Wake vortex X-band radar monitoring: Paris-CDG airport 2008 campaign results & prospectives, in: Radar'09, Bordeaux, October 2009.
[35] F. Barbaresco, Senseur multi-usage autonome, agile et cognitif : les radars multi-mission de nouvelle génération, Gestion de la complexité et de l'information dans les grands systèmes critiques, éditions SEE-CNRS, Janvier 2009.

[36] F. Barbaresco, Innovative tools for radar signal processing based on Cartan's geometry of SPD matrices and information geometry, in: IEEE International Radar Conference, Rome, May 2008.
[37] F. Barbaresco, Interactions between symmetric cone and information geometries: Bruhat–Tits and Siegel spaces models for high resolution autoregressive Doppler imagery, in: ETVC'08 Conf., Ecole Polytechnique, Nov. 2008, in: Lecture Notes in Computer Science, vol. 5416, Springer, February 2009.
[38] F. Barbaresco, G. Bouyt, Espace Riemannien symétrique et géométrie des espaces de matrices de covariance : équations de diffusion et calculs de médianes, in: GRETSI Conference, Dijon, September 2009.
[39] G. Winckelmans, F. Barbaresco, et al., The ATC-Wake Predictor system and its potential use to increase the capacity at airports, in: JISSA Conf., Paris, France, 20–21 June 2005.
[40] F. Barbaresco, et al., ATC-WAKE system design and evaluation, Technical report D2_12, European ATC-WAKE Study, IST-2001-34729.
[41] L. Spiejker, F. Barbaresco, et al., ATC-WAKE: Integrated wake vortex safety and capacity system, Technical report D6_2, European ATC-WAKE Study, IST-2001-34729.
[42] L.J.P. Speijker, F. Barbaresco, M. Frech, A. Vidal, G. Winckelmans, H. Barny, ATC-Wake: Integrated wake vortex safety & capacity system, Journal of Air Traffic Control 49 (1) (April 2007) 17–32.
[43] D. Grésillon, C. Honoré, Collective light scattering: An introduction, in: Lars Lading, et al. (Eds.), Optical Diagnostics for Flow Processes, Plenum, New York, 1994, pp. 229–243.